# Sensitivity Analysis of Railpad Parameters on Vertical Railway Track Dynamics

Maider Oregui[1]; Alfredo Núñez[2]; Rolf Dollevoet[3]; and Zili Li[4]

**Abstract:** This paper presents a sensitivity analysis of railpad parameters on vertical railway track dynamics, incorporating the nonlinear behavior of the fastening (i.e., downward forces compress the railpad whereas upward forces are resisted by the clamps). For this purpose, solid railpads, rail-railpad contact and preloaded springs are defined in a three-dimensional (3D) finite-element track model. In addition, railpads are modeled as Prony series so that measured frequency-dependent railpad properties for different clamp toe load, temperature, aging, and railpad type are considered. Through sensitivity analysis using time-domain and frequency-domain responses, the influence of the railpad parameters on the global track response is investigated. Railpad type, toe load and aging are identified as the most relevant parameters in the frequency range of 300–3,000 Hz. Furthermore, the information obtained over track response changes due to fastening loosening and railpad wear could be used for monitoring the condition of fastenings. **DOI: 10.1061/(ASCE)EM.1943-7889.0001207.** 

**Author keywords:** Vertical railway track dynamics; Frequency dependent railpad properties; Fastening; Sensitivity analysis; Finite-element model.



## Introduction

In railway transport, fastenings are fundamental track components because (1) clamps fix the rail to the support so that it stays attached to the sleeper under heavy train loads; and (2) railpads reduce the noise and vibration by adding global vertical flexibility without reducing track strength. Whereas clamps have barely been studied, railpads have widely been investigated [see a review in Sol-Sánchez et al. (2015)]. Results show that railpads play an important role on the load distribution to sleeper and ballast (Fermer and Nielsen 1995; Zakeri and Xia 2008), development of corrugation (Ilias 1999), rolling noise (Thompson and Vincent 1995), and impact loads at switches and crossings (Palsson and Nielsen 2015), transition zones (Zakeri and Ghorbani 2011) and at insulated rail joints (Mandal et al. 2016). These studies gave an initial insight into the influence of the railpad stiffness on the track dynamics. However, an in-depth analysis of the effect of different fastening parameters on the global response has not yet been reported, to the best of the authors' knowledge.

In view of the substantial influence of railpads on the railway track dynamic behavior, a mayor effort has gone into obtaining accurate railpad properties. For such purpose, the NEN-EN 13146-9 standard was released in 2011 [European Committee for Standardization 2012 (CEN 2012)]; see, for instance, its application for recycled rubber railpads in Sol-Sánchez et al. (2014). Moreover, different railpad tests have also been developed over the years. In some test studies, the nonlinear effect of preload on railpad stiffness was derived and static-load-deflection curves were defined (Thompson et al. 1998). In others, the frequency-dependent behavior of railpads was obtained for different preloads finding the dependence to preload significant whereas the dependency to frequency weaker (Thompson et al. 1998; Knothe and Yu 2001; Maes et al. 2006). In addition, the influence of temperature and aging on railpad properties was investigated and the results showed that environmental aging has a smaller influence on the mechanical performance of railpads than longer operational life (Carrascal et al. 2007; Kim et al. 2015). Considering these four relevant parameters (i.e., preload, frequency, temperature, and aging), the dynamic properties of railpads were obtained in a wide frequency range in Oregui et al. (2016a). For instance, FC9 railpads become softer after 10 years of service and their dynamic stiffness is three times larger at 2,840 Hz than at 1 Hz for a temperature of 26°C and a preload of 18 kN.

Once the dynamic behavior of railpad is better understood, the next step is to study how it affects the track response. For reproducing track dynamics, track models with different railpad representations can be found in the literature (Castellani et al. 1998; Chen and Huang 2003). Although one linear spring in series with a linear damper is commonly used, it is not a suitable model to perform a detailed analysis of fastening parameters. First of all, recent studies have shown that both the lateral (i.e., sleeper's length direction) and longitudinal (i.e., rolling direction) dimensions of the railpad influence the global response (Ferrara et al. 2013; Zhao et al. 2014; Oregui et al. 2015b). Thus, the rail seat area should be modeled to correctly reproduce track dynamics. Second, the model should consider the nonlinear behavior of the fastening, that is downward forces compress the rail and upward forces are resisted

[1]Postdoctoral, Section of Railway Engineering, Delft Univ. of Technology, Stevinweg 1, 2628 CN, Delft, Netherlands. E-mail: M.Oregui@tudelft.nl

[2]Researcher and Docent, Section of Railway Engineering, Delft Univ. of Technology, Stevinweg 1, 2628 CN, Delft, Netherlands (corresponding author). ORCID: http://orcid.org/0000-0001-5610-6689. E-mail: A.A.NunezVicencio@tudelft.nl

[3]Full Professor, Section of Railway Engineering, Delft Univ. of Technology, Stevinweg 1, 2628 CN, Delft, Netherlands. E-mail: R.P.B.J.Dollevoet@tudelft.nl

[4]Associate Professor, Section of Railway Engineering, Delft Univ. of Technology, Stevinweg 1, 2628 CN, Delft, Netherlands. E-mail: Z.Li@tudelft.nl

Note. This manuscript was submitted on February 23, 2016; approved on October 4, 2016; published online on February 1, 2017. Discussion period open until July 1, 2017; separate discussions must be submitted for individual papers. This paper is part of the ***Journal of Engineering Mechanics***, © ASCE, ISSN 0733-9399.

by the clamps. In this manner, the effect of railpad stiffness and clamp preload (called toe load) can be differentiated. Last, the dynamic properties of railpads should be accounted for in the model because they may significantly change with frequency (Oregui et al. 2016a).

In this paper, a 3D finite-element (FE) model is defined with frequency-dependent railpads and preloaded clamps. Solid railpads cover the entire rail seat, contact is defined between rail and railpad, and rails are fixed to the sleeper by preloaded springs. The current model is an improvement of the one presented in Oregui et al. (2015b) because railpads are defined as Prony series instead of as elastic. In this manner, the frequency-dependent behavior of railpads is explicitly included in the model. With such a 3D FE model, a sensitivity analysis of the fastening parameters on the track dynamics is performed. The measured dynamic properties of FC9 railpads at different temperatures, toe loads and aging from (Oregui et al. 2016a) are introduced into the new proposed 3D FE model and the results are analyzed. To complete the study, how the railpad type influences the track dynamics is investigated as well. In addition, the use of the findings for monitoring fastening degradation is discussed.

## Methodology

### 3D Finite-Element Model

A 3D finite-element track model with frequency-dependent railpads is developed (Fig. 1) and its dynamics are studied by numerically simulating hammer tests. A 24 sleeper bays long whole track is modeled, which is a suitable length for reproducing hammer tests (Oregui et al. 2016b). The UIC54 rails are modeled according to their nominal geometry using solid elements. The rail inclination is 1:40 and the rail ends are clamped. The rails are defined as elastic; this is suitable because hammer loads do not cause plastic deformation. The NS90 sleepers are also modeled according to their nominal geometry and as elastic, which is considered a suitable material model for the loads investigated (Gustavson and Gylltoft 2002).

The ballast consists of multiple linear spring and viscous damper pairs homogeneously distributed under the sleeper. The lateral stiffness of the ballast is considered by fixing the ballast nodes connected to the sleepers in the lateral direction of the track (i.e., $y$ direction in Fig. 1) (Oregui et al. 2016b). The ballast lower nodes are fixed in all three directions. Lower layers (e.g., subballast and foundation) are not considered because their influence on the vertical track dynamics is negligible in the frequency range of interest of this paper (i.e., 300–3,000 Hz) (Knothe and Wu 1998).

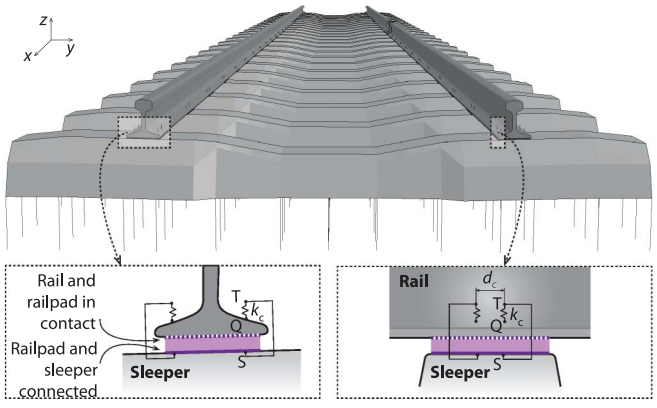


**Fig. 1.** 3D FE track model with closeups of the fastening model

The fastening system is represented via its two main components: railpad and clamps. The railpad is modeled with solid elements covering the entire rail seat. The lower surface is connected to the sleeper whereas surface-to-surface contact with Coulomb friction is defined between the rail and the upper surface of the railpad (see left closeup in Fig. 1). A friction coefficient $\mu$ of 0.75 is assumed (Oregui et al. 2015b) and the penalty method (Benson and Hallquist 1990) is employed for the contact calculation. By defining contact, relative movement between rail and railpad may occur and the nonlinear behavior of the fastening is considered. FC9 railpads, commonly used in mainlines in the Netherlands, are modeled. The Prony series is used as material model (Fig. 2) so that frequency-dependent stiffness and damping are considered. The Prony series is defined in the time domain as (Biot 1954):

$$E(t) = \frac{\sigma(t)}{\varepsilon_0} = E_\infty + \sum_{j=1}^{n} E_j e^{-t/\tau_j} \tag{1}$$

where $E_\infty$ = stiffness of the spring in parallel; $E_j$ = stiffness of the spring $j$; $\tau_j$ = ratio $\eta_j/E_j$ known as the relaxation time constant of the term $j$; $\eta_j$ = viscosity of the damper $j$; and $n$ = number of terms. The number of terms required to accurately model a given material response is determined based on the quality of the fitting of the measured response data. The values of the Prony series parameters used in this paper are presented later.

To fix the rail to the support, clamps are modeled. Each clamp consists of two preloaded springs separated a distance $d_c$ in the longitudinal direction of the rail, which is the distance between the acting points of a clamp on the rail (see right closeup in Fig. 1). This distance $d_c$ is assumed to be 72 mm (Oregui et al. 2015b). The fixing of the clamp to the sleeper is represented by coupling in the $x$, $y$, and $z$ directions the upper node of the spring ($T$) and its vertical projection on the sleeper ($S$) (see closeups in Fig. 1). Moreover, the lateral constraint that the base plate of the fastening system applies on the rail and railpad is represented by coupling the upper and lower nodes of the spring ($T$ and $Q$, respectively) in the $y$ direction of the rail. The springs are preloaded to consider the toe load $F_{TL}$ that clamps apply on the rail in the field. In the model, the toe load is considered by defining an initial displacement of the springs $\Delta l$ as follows:

$$\Delta l = \frac{F_{TL}}{k_c} \tag{2}$$

where $k_c$ = stiffness of the clamp. The toe load is divided equally between the two springs of a clamp.

Table 1 summarizes the track parameters. For the rail and sleeper, nominal values are used. The ballast stiffness and damping are obtained by fitting simulations to a set of field measurements (Oregui et al. 2015a) and the clamp parameters are taken from

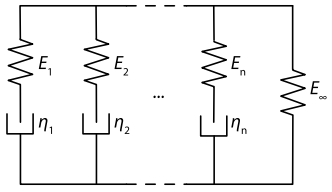


**Fig. 2.** Prony series railpad model to account for frequency-dependent properties

**Table 1.** Track Parameters

| Component | Parameter | Value |
|---|---|---|
| Rail, UIC54 | Young's modulus, $E_r$ | 210 GPa |
| Rail, UIC54 | Density, $\rho_r$ | 7,800 kg/m$^3$ |
| Rail, UIC54 | Poisson's ratio, $\nu_r$ | 0.3 |
| Sleeper, NS90 | Young's modulus, $E_s$ | 39 GPa |
| Sleeper, NS90 | Density, $\rho_s$ | 2,480 kg/m$^3$ |
| Sleeper, NS90 | Poisson's ratio, $\nu_s$ | 0.2 |
| Sleeper, NS90 | Sleeper span | 0.6 m |
| Clamp, Skl 14 | Stiffness, $k_c$ | 800 kN/m |
| Clamp, Skl 14 | Spring distance, $d_c$ | 72 mm |
| Clamp, Skl 14 | Friction coefficient, $\mu$ | 0.75 |
| Ballast | Stiffness, $k_b$ | 45 MN/m |
| Ballast | Damping, $c_b$ | 96 kNs/m |

(Oregui et al. 2015b). The railpad data is presented later in this section.

Some clarifications about the proposed 3D Model are as follows:

- Regarding the validity of the 3D model, the track components were modeled so that their dynamic behavior was represented good enough in the frequency range of interest (300–3,000 Hz). For instance, the rail is represented with 3D solid elements to account for its modes and vibrations, whereas the ballast is represented with spring-damper pairs because it is not one of the dominant contributors in the frequency range of interest. The model was validated in the range 300–3,000 Hz using hammer test measurement, as explained in the next subsection. Seven characteristics in the receptance function are the most relevant and they are all captured by the model (Oregui et al. 2015b).
- The model proposed in this paper is valid between 300 and 3,000 Hz. Particularly, the frequencies below 300 Hz are not sufficiently excited by the hammer, and they are the ones related to the dynamics of the ballast and subgrade (Grassie et al. 1982; Wu and Thompson 2000), and thus out of the scope of this paper. Regarding the friction between railpad and sleeper, a more detailed definition of the ballast would be required to account for the friction (Sadeghi 2010; Kumaran et al. 2003).
- About the boundary conditions, for the railpads its lower surface is connected to the sleeper. The upper surface is in contact with the rail, and coulomb friction is defined. There are no other boundary conditions for the railpads. The nodes are not coupled, or fixed displacements are not defined.
- For the fastening, two springs per clip are considered, thus two springs on each side of the rail. The upper and lower nodes of the spring are coupled on the lateral and longitudinal directions. The upper node is also coupled in all three directions with the projection node on the sleeper. In this way, the rail can vertically move relative to the railpad, so the function of the clip is reproduced.

For obtaining the dynamic behavior of the track, hammer tests are numerically calculated combining *ANSYS* and *LS-Dyna*. First, the equilibrium state of the track is calculated with *ANSYS* applying the implicit FE approach. Next, hammer tests are simulated in the time domain with *LS-Dyna* applying the explicit FE approach. Time domain calculations are required to account for the nonlinearity of contact between rail and railpad and the frequency-dependent behavior of railpads.

### Hammer Test

The hammer excitation is applied on the rail over the sleeper (i.e., on-support). The excitation on the rail between sleepers (i.e., midspan) is not simulated because the influence of the fastening on the vertical track dynamics is more clearly observed on the on-support configuration due to proximity to the fastening. In the simulation, the impact is defined as a triangular force of stating time $t_0$, maximum force time $t_1$, finishing time $t_2$, and maximum force $F_{\max}$. The values for the impact load are fitted from the field measurements. The simplification of hammer excitation to a triangular force is suitable for investigating vertical track dynamics (Oregui et al. 2016b). Simulations were run with the real shape and the triangular shape, and the differences were negligible. The values of $t_0$, $t_1$, $t_2$, and $F_{\max}$ can easily be obtained from measurements. In this paper, $t_0$, $t_1$, and $t_2$ are 0, 0.25, and 0.4 ms, respectively, and $F_{\max}$ is 3,097 N.

Once the impact is applied, the resulting vibration of interest is the vertical acceleration of the rail close to the excitation. According to field observations, the distance between the hammer impact and the accelerometer is approximately 2 cm (Oregui et al. 2016b). In the 3D FE model, this rail section 2 cm away from the excitation application is meshed with an element size of 1 mm so that, with a time step of $1.22 \times 10^{-7}$ s, the Courant's convergence criterion (Courant et al. 1928) is fulfilled during the explicit calculation.

In the hammer-test measurement conducted, the time domain averaged force and acceleration response of five impacts are considered as in Oregui et al. (2015c). The average is done by matching the maximum peaks of the signals. Then, to simplify the simulation, the real-life averaged response was fitted into a triangular shape measurement force values. Once the track response to hammer excitation is obtained, the next step is to extract information (e.g., characteristic frequencies) from the numerically calculated signals. For this purpose, the input force $F(t)$ and output acceleration $a(t)$ are transformed into the frequency domain by means of fast Fourier transform and then the receptance function $H(f)$ is calculated as follows:

$$H(f) = \frac{1}{(2\pi f)^2}\frac{S_{aF}(f)}{S_{FF}(f)} = \frac{1}{(2\pi f)^2}\frac{\sum_{n=1}^{N}\sum_{m=1}^{N-m-1} a[m+n]F[m]e^{-i2\pi fn}}{\sum_{n=1}^{N}\sum_{m-1}^{N-m-1} F[m+n]F[m]e^{-i2\pi fn}} \quad (3)$$

where $f$ = frequency; $S_{aF}$ = cross spectrum between the force and the acceleration; and $S_{FF}$ = autospectrum of the force.

Fig. 3 shows the measured mean receptance function of a set of field hammer tests measurements in the valid frequency range of 300–3,000 Hz (Oregui et al. 2015a). The 21 reference locations did not show visible damage and were combined to consider the intrinsic variability of the track structure. In addition to the measured mean and the two standard deviations with respect to the mean, Fig. 3 shows the seven main characteristics of tracks with monoblock sleepers: second bending mode of the sleeper (M1), the in-phase rail resonance (M2), the antiphase rail resonance (M3), the pin-pin antiresonance (M4), the fourth bending mode of the sleeper (M5), the second-order pin-pin antiresonance (M6), and the 2,000 Hz resonance (M7) (Grassie et al. 1982; Oregui et al. 2016b).

### Laboratory Test of the Frequency-Dependent Railpad Properties

The laboratory test were carried out following the procedure proposed in Oregui et al. (2016b), making use of the time-temperature superposition principle, in which the dynamic properties of a material can be determined in a broad frequency domain by changing the temperature. First, the dynamic behavior of railpads is measured at different frequencies. Next, assuming that the dynamic

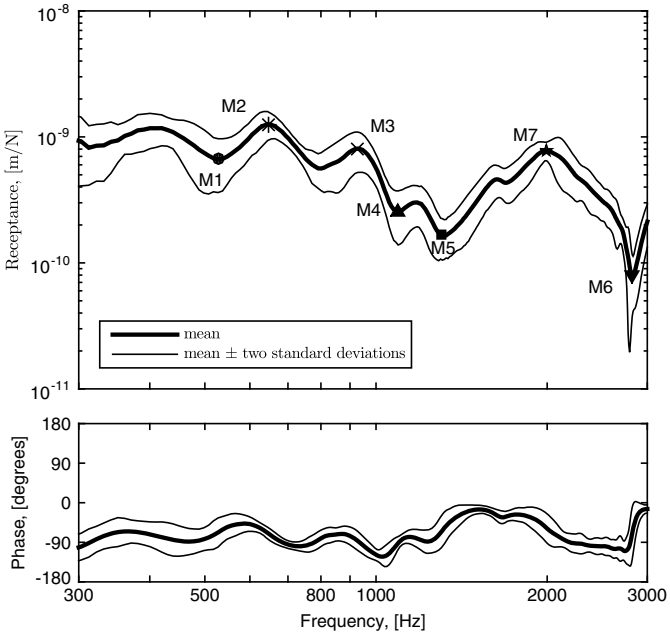


**Fig. 3.** Measured on-support track vertical receptance function; the characteristics are the second bending mode of the sleeper (M1), the in-phase rail resonance (M2), the antiphase rail resonance (M3), the pin-pin antiresonance (M4), the fourth bending mode of the sleeper (M5), the second-order pin-pin antiresonance (M6), and the 2,000 Hz resonance (M7)

behavior at lower temperatures resembles the behavior at higher frequencies, the curves are shifted using the Williams-Landel-Ferry (WLF) relation (Williams et al. 1955).

Thus, frequency-dependent behavior of FC9 railpads under different preloads and temperatures were obtained by combining dynamic mechanical analysis (DMA) measurements and the time-temperature superposition principle. First, railpads were tested under dynamic loads at different frequencies, temperatures, and preloads. In the tests, the frequencies were 1, 3, 5, 8, 10, 20, 40, and 60 Hz; the preloads were 6, 12, and 18 kN; and the temperatures were 26, 10, 0, and −10°C. Next, the measured curves were shifted in frequency by applying the time-temperature superposition principle so that a frequency range wider than the tested frequency range was covered (Williams et al. 1955; Christensen 1982). The resulting curves are called master curves, and the final frequency range is determined by the number of temperatures tested and the temperature dependency of the material. For instance, in the case of new FC9 railpads, the dynamic behavior could be obtained up to 2,840 Hz for a temperature of 26°C.

The measured dynamic behavior can be displayed, for instance, as complex dynamic modulus $E^*$ (viscoelastic behavior), loss modulus $E''$ (viscous behavior), or storage modulus $E'$ (elastic behavior) (Ferry 1961). The three entities are related as follows:

$$E^*(\omega) = E'(\omega) + iE''(\omega) \tag{4}$$

$$|E^*(\omega)| = \sqrt{[E'(\omega)]^2 + [E''(\omega)]^2} \tag{5}$$

where $\omega = 2\pi f$; and $f$ = frequency.

These moduli are fundamental to model materials as Prony series. More precisely, measured storage and loss moduli are fitted in order to derive the values of the stiffness $E_j$ and viscosity $\eta_j$ of the Prony series, see Eq. (1). The fitting between the measurements and numerical material model is performed in the frequency domain by minimizing the error between the measured storage modulus $E'$ and the loss modulus $E''$, and the modeled storage modulus $E'_{\text{prony}}$ and loss modulus $E''_{\text{prony}}$, respectively:

$$\begin{aligned}&\min[(E' - E'_{\text{prony}})^2 + (E'' - E''_{\text{prony}})^2] \\ &= \min\left\{\left[E' - \left(E_\infty + \sum_{j=1}^{n} \frac{E_j \omega^2 \tau_j^2}{1 + \omega^2 \tau_j^2}\right)\right]^2 \right. \\ &\left. + \left[E'' - \left(\sum_{j=1}^{n} \frac{E_j \omega \tau_j}{1 + \omega^2 \tau_j^2}\right)\right]^2\right\}\end{aligned} \tag{6}$$

As an example, the Prony series parameters for a new FC9 railpad are summarized in Table 2. Less terms are required to reproduce the master curves of 10 and 0°C than the master curve of 23°C because the frequency range obtained for 10 and 0°C is narrower than the frequency range obtained for 23°C.

By analyzing the master curves, one can see that the complex modulus increases with increasing preload and frequency. The influence of frequency is determined by the dependency of the material on temperature and this is directly related to the damping capacity of the material. For instance, contrary to new FC9 railpads, a low maximum frequency is obtained for worn FC9 railpads because damping behavior of the material has decreased to nearly nonexistent. The influence of the preload is significant and nonlinear for the materials tested in (Oregui et al. 2016b) and investigated in this paper.

## Numerical Results: Sensitivity Analysis

First, the effect of defining frequency-dependent railpads on track vibrations is studied. Next, the vertical track dynamics are investigated for FC9 railpads at several temperatures, toe loads, and ages using the 3D FE model with frequency-dependent railpads. In addition, the vertical track dynamics for other railpad types are studied. In every case investigated, the measured dynamic stiffness of three railpads is used so that the variation between samples is considered.

**Table 2.** Prony Series Coefficients for a New FC9 Railpad for Different Preloads and Temperatures

| Relaxation time, parameter | Relaxation time, value (s) | Stiffness, parameter | Stiffness, preload 18 kN, 23°C (MPa) | Stiffness, preload 12 kN, 23°C (MPa) | Stiffness, preload 6 kN, 23°C (MPa) | Stiffness, temperature 10°C, 18 kN (MPa) | Stiffness, temperature 0°C 18 kN (MPa) |
|---|---|---|---|---|---|---|---|
| — | — | $E_\infty$ | 133 | 90 | 56 | 170 | 190 |
| $\tau_1$ | 0.1 | $E_1$ | 63 | 44 | 14 | 60 | 70 |
| $\tau_2$ | 0.01 | $E_2$ | 50 | 40 | 20 | 100 | 120 |
| $\tau_3$ | 0.001 | $E_3$ | 80 | 70 | 23 | 90 | 60 |
| $\tau_4$ | 0.0001 | $E_4$ | 41 | 80 | 40 | — | — |

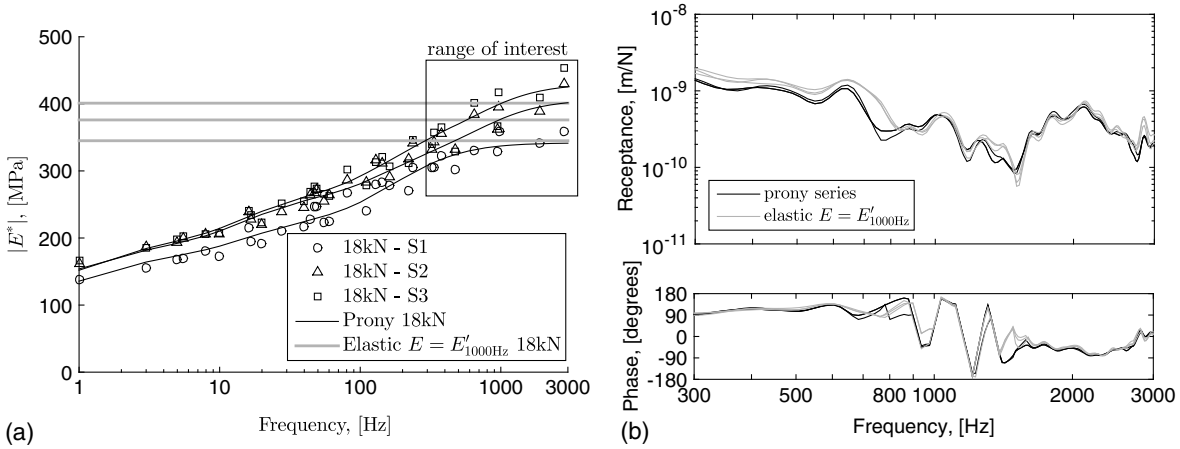


**Fig. 4.** New FC9 railpads at a toe load of 18 kN and a temperature of 26°C: (a) measured railpad dynamic properties (S: sample) and elastic and Prony series models; (b) simulated vertical track response

### *Frequency Dependency*

Fig. 4(a) displays the Prony series fitted to the measured dynamic railpad stiffness of new FC9 railpads for a toe load of 18 kN at a temperature of 26°C. Moreover, the figure includes the frequency-independent models (i.e., elastic models) whose Young's modulus $E$ corresponds to the storage modulus $E'$ of the Prony series at 1,000 Hz (i.e., $E'_{1000\ \mathrm{Hz}}$). By introducing the two material models in the 3D FE model, how the frequency-dependent behavior of railpads affect the vertical track dynamics is investigated.

Fig. 4(b) shows the resulting track receptance functions when frequency-dependent and frequency-independent railpads are defined. Only small differences are found between the vertical track response with railpads modeled as Prony series or elastic. The curves disagree primarily at the low frequencies of the frequency range of interest because the difference between the measured railpad stiffness in the low frequency and the assumed constant railpad stiffness $E = E'_{1000\ \mathrm{Hz}}$ seems to be big enough (13%) to influence the receptance value of the track response. However, the change in characteristic frequencies such as the rail resonances at approximately 645 and 1,035 Hz is negligible. Thus, in order to numerically reproduce the dynamic response of a track, the frequency-dependent behavior of railpads can be considered in the frequency range 300–3,000 Hz by defining a Young's modulus $E$ equivalent to the storage modulus $E'$ at 1,000 Hz (i.e., $E = E'_{1000\ \mathrm{Hz}}$). The increase in magnitude at low frequencies could be accepted in exchange for reducing the calculation time because a linear material model is defined instead of a time-consuming nonlinear material model.

### *Temperature*

The measured dynamic behavior of new FC9 railpads at 26, 10, and 0°C for a toe load of 18 kN are shown in Fig. 5(a). The frequency range obtained after the time-temperature superposition is wider at 26°C than at 10 and 0°C (Oregui et al. 2016a). Consequently, the measured dynamic behavior at 10 and 0°C is partly unknown in the frequency range of 300–3,000 Hz. To overcome this limitation, the corresponding Prony series were extended with one more term by assuming almost no increase in stiffness. On the basis of the previous results, this modeling approximation is suitable at 10°C. However, at 0°C the stiffness at low frequencies is reasonably defined, whereas the stiffness at high frequencies may be underestimated.

Fig. 5 displays the receptance functions for the three different temperatures. This study did not consider changes in the rail or

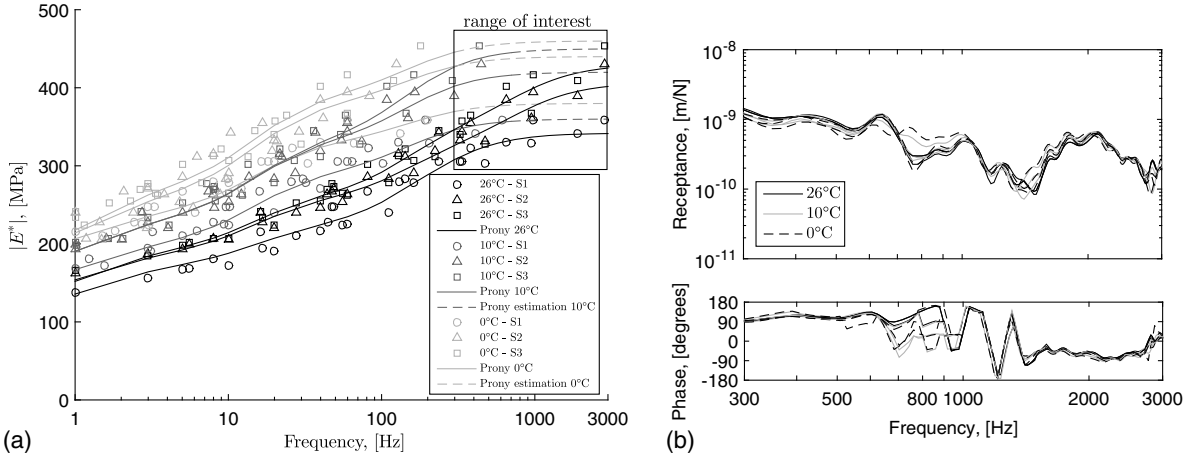


**Fig. 5.** New FC9 railpads for a toe load of 18 kN at different temperatures, 26, 10, and 0°C: (a) measured railpad dynamic properties (S: sample) and Prony series models; (b) simulated vertical track response

clamping system (e.g., shrinking or expansion of steel) due to temperature variation; only railpad properties were changed. Although the resulting phase angles are dispersed between 600 and 900 Hz, the receptance functions are almost identical, except for two curves which correspond to the railpad with significantly smaller stiffness than the others at 10 and 0°C [Fig. 5(a)]. Thus, the changes in FC9 railpad properties due to temperature do not influence significantly the track vertical response. In the field, this means that measurements performed during the day (hot) and night (cold) will not significantly vary because of railpad property variation caused by the temperature change.

### Toe Load

Fig. 6(a) shows the measured dynamic behavior of new FC9 railpads for toe loads of 18, 12, and 6 kN at 26°C. In the Netherlands, the nominal toe load is 20 kN. Thus by considering smaller toe loads, one can study how clamp loosening affects the vertical track dynamics. For this purpose, Prony series were fitted to the measurements in Fig. 6(a) and the initial displacement of the clamps were calculated according to Eq. (2) for each toe load. The input data was introduced in the 3D FE model and hammer tests were numerically calculated. The resulting vertical track dynamics are shown in Fig. 6(b).

If the toe load decreases from 18 to 12 kN, the primary difference between the receptance functions is the shift to lower frequencies of the antiphase rail resonance (peak at 900–1,000 Hz) and the fourth bending mode of the sleeper (deep at 1,300–1,500 Hz). These two changes can be explained as follows. In the antiphase rail resonance, the rail vibrates in antiphase to the sleeper so that, if the connection between rail and sleeper is loosed, the characteristic mode occurs at a lower frequency. Regarding the fourth bending mode of the sleeper, if the fastening of the sleeper to the rail changes, the characteristic frequencies of the sleeper change (Kaewunruen and Remennikov 2006); a more flexible rail-sleeper connection results in lower characteristic frequencies.

Defining a toe load as low as 6 kN brings significant changes to the vertical track dynamic behavior. The connection between rail and sleeper is so loose than the rail-sleeper interaction changes. The antiphase rail resonance occurs at a similar frequency than the inphase rail resonance, which explains the increase in the value of the peak at approximately 625 Hz. In addition, the fourth bending mode of the sleeper is not transmitted to the rail so that it disappears from the track dynamic response measured at the rail; see the receptance and phase in the frequency range of 1,300–1,500 Hz in Fig. 6(b). Besides changes in the vertical track dynamics, for frequencies higher than 1,500 Hz the curves show a trend toward lower frequencies if the toe load decreases. The maximum found at 2,000 Hz for a toe load of 18 kN shifts to lower frequencies for smaller toe loads. This change was expected as the fastening is one of the dominant track components that define the track response in these frequencies (Oregui et al. 2015b).

### Aging

Worn railpads were removed from the Woerden-Utrecht line in the Netherlands after 10 years, in which they withstood 60 million gross tons. Fig. 7(a) shows their measured dynamic stiffness at 26°C for toe loads of 18, 12, and 6 kN. The spread of the measurements for the toe load of 18 kN is most probably because the geometrical differences of the samples affect the loading condition, and consequently, the measured stiffness (Oregui et al. 2016a). Under the same test conditions, the maximum frequency for worn FC9 railpads is significantly lower than for new FC9 railpads (i.e., 200 versus 2,840 Hz). The difference is because worn FC9 railpads lost most of their damping capacity (Oregui et al. 2016a). This means that their dynamic behavior is weakly dependent on temperature, and by applying the time-temperature superposition (Christensen 1982) also weakly dependent on frequency. Therefore, defining a constant stiffness in the frequency range of 300–3,000 Hz for the worn FC9 railpads tested is a suitable assumption. The Young's modulus $E$ assumed was the largest measured storage modulus (i.e., $E'_{200\ \mathrm{Hz}}$).

New and old railpads were used in the laboratory. They were tested under the same preload by squeezing them until the desired preload was obtained. Because the worn rail pads are thinner than the new ones, the distance between the plates was smaller in worn railpads case. In the controlled lab test with the same preload/pressure on the rail pads, the old pads showed lower stiffness. However, in the real-life field old rail pads are worn and thus thinner so the clips are looser and preload is lower. This could lead to an unreal lower stiffness of the railpads.

Vertical track dynamics with worn and new FC9 railpads are compared for toe loads of 18, 12, and 6 kN in Figs. 7(b–d), respectively. For the three preloads, the same trend is observed: some characteristics of the track receptance function shift to lower frequencies when worn FC9 railpads are defined instead of new FC9 railpads. The frequencies of (1) the antiphase rail resonance (900–1,000 Hz);

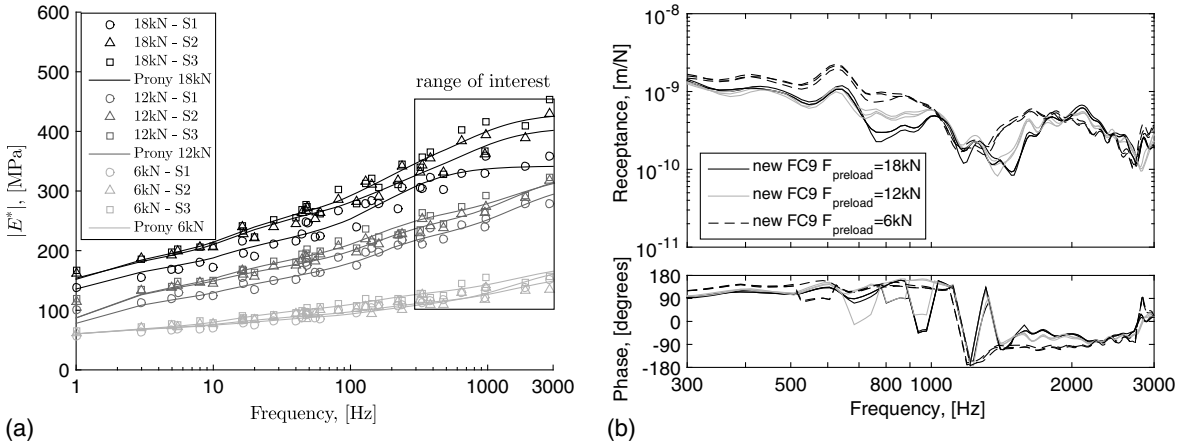


**Fig. 6.** New FC9 railpads at a temperature of 26°C for different toe loads, 18, 12, and 6 kN: (a) measured railpad dynamic properties (S: sample) and Prony series models; (b) simulated vertical track response



J. Eng. Mech., 2017, 143(5): 04017011

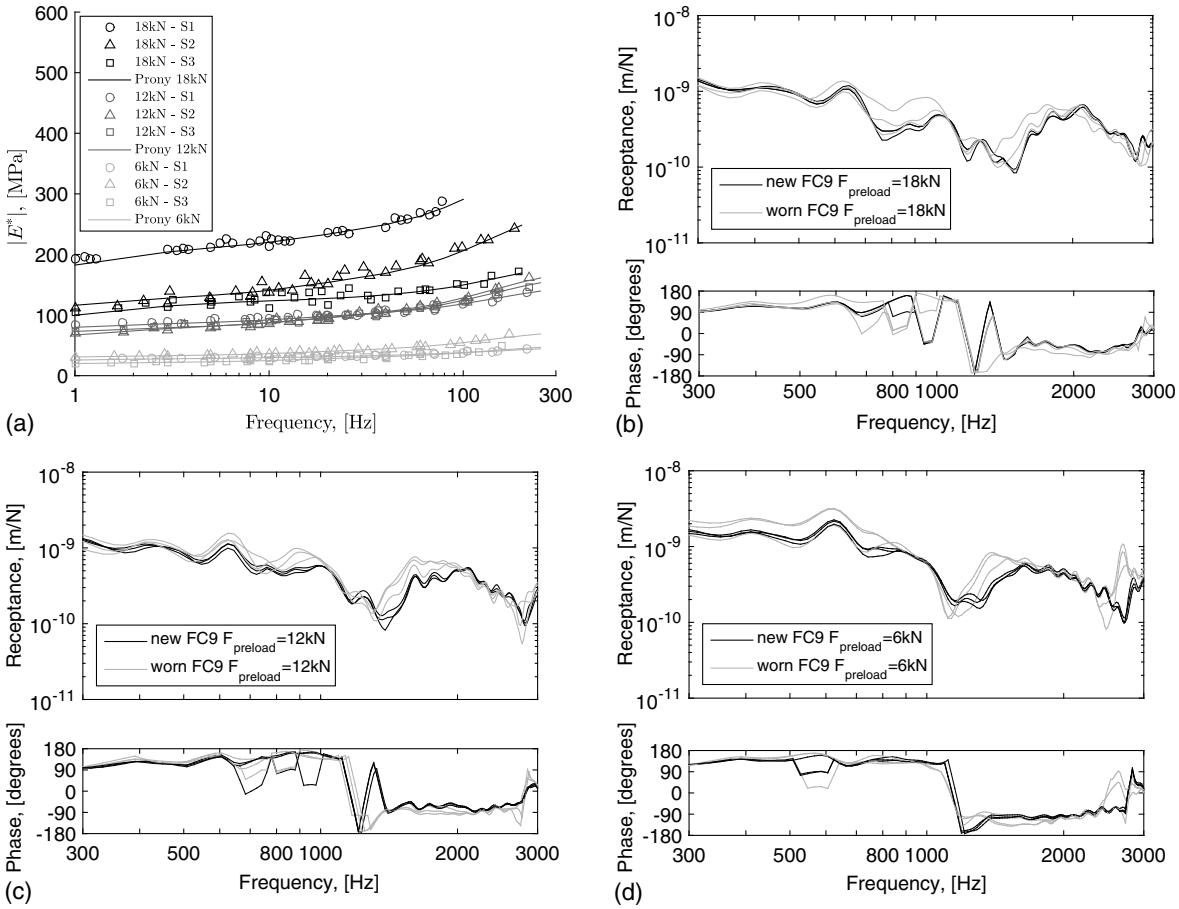


**Fig. 7.** Worn FC9 railpads at 26°C for different toeload, 18, 12, and 6 kN: (a) Prony series and simulated vertical track response; (b) 18 kN; (c) 12 kN; (d) 6 kN

(2) the fourth bending mode of the sleeper (1,300–1,500 Hz); and (3) the maximum in the frequency range of 1,500–2,500 Hz decrease with railpad wear. As in the toe load study of sub-section "Toe Load," these characteristic frequencies change because a worn FC9 railpad is less stiff than a new FC9 railpad for the same temperature and preload. Consequently, the rail support is more flexible so that (1) the antiphase vibration between rail and sleeper occurs at lower frequency; (2) the characteristic frequencies of the sleeper decrease (Kaewunruen and Remennikov 2006); and (3) the track vibration dominated by the fastening occurs at lower frequencies (Oregui et al. 2015b). Another effect of railpad wear on track vertical dynamics is that the receptance function increases for frequencies below 1,000 Hz, which means that the displacement is larger, and therefore more energy concentrates at these frequencies.

### *Different Railpad Types*

Besides FC9 railpads, FC1530 and Orange railpads are investigated. Both FC1530 and FC9 railpads are made of polyurethane cork rubber, but the cork content in FC1530 railpads is higher than in FC9 railpads. Orange is a recently developed material designed for the absorption of short, intensive dynamic loads and vibrations, and it is suitable for railway use.

The measured dynamic behavior of FC1530 railpads is shown in Fig. 8(a). The obtained frequency range does not cover the entire frequency range of interest. Thus, as in the temperature study, one more term is added to the Prony series so that the stiffness slightly increases with frequency. This approach is taken because the results of previous section show that, for vertical track dynamics, the frequency-dependent dynamic behavior of FC9 railpads between 300 and 3,000 Hz can reasonably be defined by the dynamic behavior at 1,000 Hz. FC1530 railpads are less temperature-dependent, and therefore less frequency-dependent than FC9 railpads. Thus, slightly increasing the dynamic behavior after 600 Hz based on the curve between 300 and 600 Hz is a suitable estimation. In the 3D FE model, FC1530 railpads are defined with the Prony series of Fig. 8(a), a Poisson's ratio of 0.4, and a density of 1,100 kg/m$^3$. Regarding Orange railpads, the material is hardly dependent on frequency (Oregui et al. 2016a). Therefore, they are defined as elastic [Fig. 9(a)] with a Poisson's ratio of 0.3, and a density of 860 kg/m$^3$.

The numerically calculated vertical dynamics of tracks with FC1530 and Orange railpads at 26°C for different toe loads are displayed in Figs. 8 and 9, respectively. At 18 kN, the receptance functions significantly differ from the receptance functions of tracks with FC9 railpads. Tracks with FC1530 and FC9 railpads show two main resonances, which are the first-order and second-order pin-pin resonances at approximately 1,050 and 2,700 Hz, respectively. In turn, tracks with FC9 railpads have seven main characteristics. The variation in dynamic track behavior is caused by the big difference in stiffness; FC1530 and Orange railpads are at least four times softer than FC9 railpads. With a softer support, the vibrations of the sleeper reach the rail attenuated so that the bending modes of the sleeper are not characteristic modes of the track response (M1 and M5 in Fig. 3). Furthermore, the interaction between the rail and sleeper is more flexible causing the in-phase and antiphase



J. Eng. Mech., 2017, 143(5): 04017011

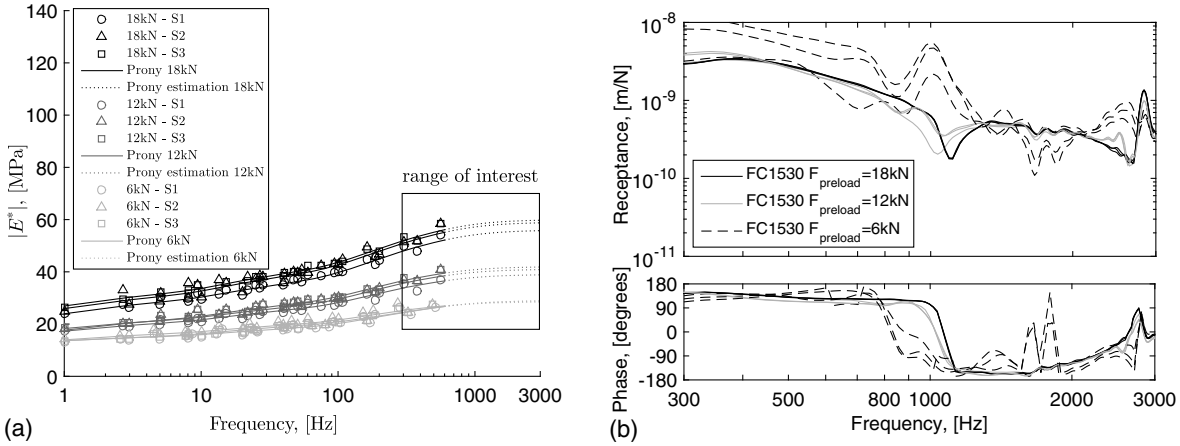


**Fig. 8.** FC1530 railpads at 26°C for different toeload, 18, 12, and 6 kN: (a) Prony series; (b) simulated vertical track response

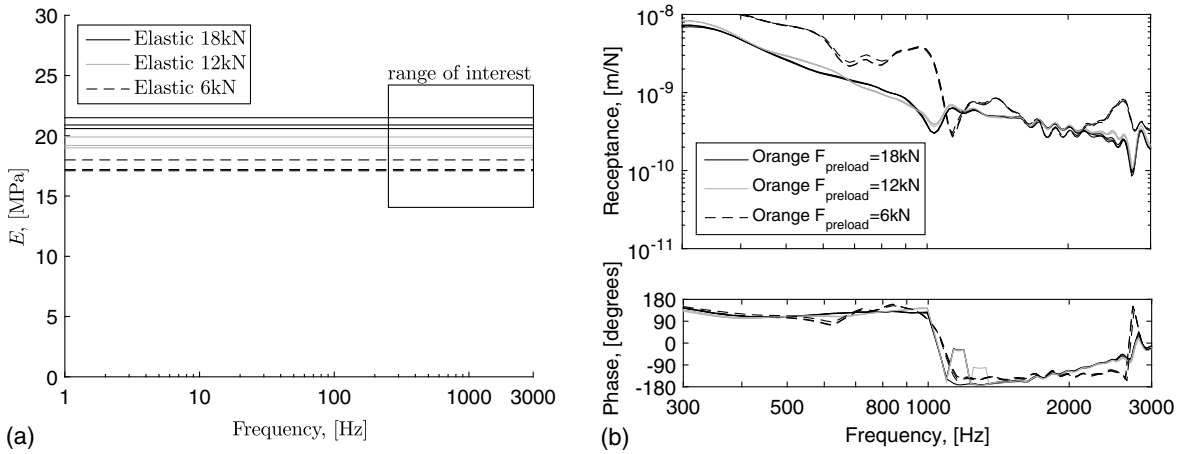


**Fig. 9.** Orange railpads at 26°C for different toeload, 18, 12, and 6 kN: (a) Young's modulus; (b) simulated vertical track response

rail resonances not to be visible in the track receptance function between 300 and 3,000 Hz (M2 and M3 in Fig. 3). In addition, the frequency range of 1,500–2,500 Hz, which is partly defined by the fastening, does not show a maximum (M7 in Fig. 3). Thus, the two characteristics that remain are the first-order and second-order pin-pin resonances (M4 and M6 in Fig. 3) because they are not greatly affected by the railpad properties, but they are primarily determined by the distance between sleepers and rail properties (Grassie et al. 1982). Softer railpads attenuate sleeper and rail vibrations on the global track response. However, according to the receptance function values, larger displacements occur in tracks with soft railpads than in track with stiff railpads and this may accelerate the fatigue of track components.

As tracks with FC9 railpads, tracks with FC1530 and Orange railpads change their dynamic behavior when the toe load is 6 kN. Energy concentrates at frequencies lower than 1,000 Hz and the dynamic behavior changes in the frequency range 1,500–2,500 Hz. These changes are observed for tracks with three railpads of very different stiffness. Thus, the difference in behavior is not caused by the downward forces compressing the rail but by the upward forces that are resisted by the clamps. This is the nonlinear behavior of the fastening and it could numerically be reproduced thanks to the contact-clamp fastening model of the current 3D FE model. On the basis of these results, one can conclude that loose fastenings (i.e., $F_{TL} \leq 6$ kN) are clearly observed on vertical unloaded track dynamics.

## Discussion: Monitoring of the Fastening Condition

The information obtained from the sensitivity analysis could be applied to monitor the condition of fastening with FC9 railpads. Under service and environmental conditions, railpads worn and clamps loosen. These two processes of railpad aging and toe load decrease are closely related. On the one hand, worn FC9 railpads become softer and thinner so that the resulting toe load is smaller than the initial toe load with new FC9 railpads. Conversely, smaller toe loads result in a smaller railpad stiffness, and consequently larger rail displacement occurs, which may accelerate the fatigue of the clamps and wear of railpads. Thus, railpad aging feeds back to toe load decrease and vice versa, and therefore fastening deterioration accelerates.

In the sensitivity analysis, the same trends were observed on the vertical track dynamics for both railpad aging and toe load decrease. Fig. 10 shows the case closest to the nominal condition (i.e., new FC9 for a toe load of 18 kN), the most deteriorated case (i.e., worn FC9 for a toe load of 6 kN), and an intermediate case (i.e., worn FC9 for a toe load of 18 kN). According to the study presented in this

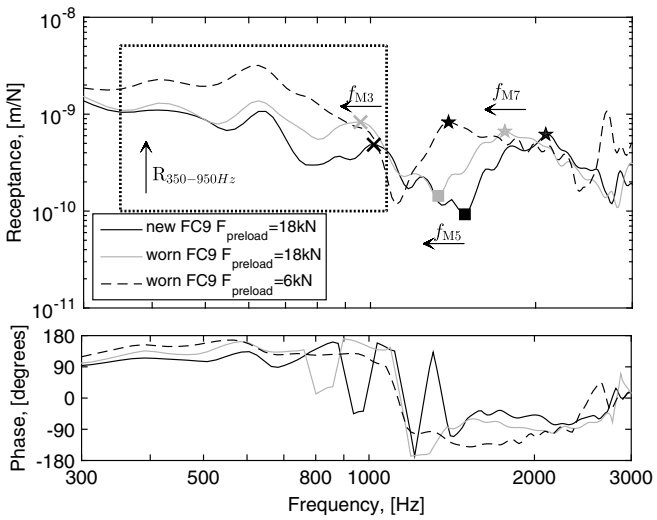


**Fig. 10.** Effect of fastening deterioration on vertical track dynamics

paper, if rails wear and/or clamps loosen then (1) the frequencies of the antiphase rail resonance $f_{M3}$, the second bending mode of the sleeper $f_{M5}$, and the maximum at 2,000 Hz $f_{M7}$ shift to lower frequencies; and (2) the receptance function for frequencies lower than 1,000 Hz increases significantly. This information could be used to monitor the condition of fastening systems by dynamic-response-based train-borne measurements systems such as axle box acceleration systems (Molodova et al. 2014; Li et al. 2015) and strain-gauge-instrumented wheelsets systems (Kassa and Nielsen 2008). Although the loading condition of the current research and train-borne measurements is different (i.e., unloaded versus loaded track), research into squat and insulated rail joint damage detection suggests that the frequencies identified by hammer test analysis may be valuable input for train-borne detection algorithms (Oregui et al. 2015a, c).

## Conclusion and Future Research

The influence of railpad parameters on the railway track response is investigated by numerically reproducing vertical track dynamics via a 3D finite-element model. The advanced fastening model defined includes solid frequency-dependent railpads in contact with the rail and clamps as preloaded springs. By introducing in the 3D FE model measured dynamic railpad properties, five main parameters of the fastening have been studied: frequency-dependency of railpads, temperature, toe load (i.e., clamping force), aging, and railpad type. According to the results:

- Variations in railpad properties due to temperature lead to negligible changes on the vertical track dynamics;
- Frequency-dependent properties of FC9 railpads can also be neglected if the railpads are defined with a Young's modulus corresponding the storage modulus at 1,000 Hz;
- Toe load, aging, and railpad type significantly affect vertical track vibrations; and
- Loosened clamps (i.e., $F_{TL} \leq 6$ kN) drastically change the global track response, whereas with tighter clamps (i.e., $F_{TL} \geq 12$ kN), the railpad type and wear contribute to determine to a large extend the track dynamics. For instance, in the current study, tracks with FC1530 and Orange railpads resulted in less characteristic modes than tracks with FC9 railpads between 300 and 3,000 Hz.

Part of the future work includes to analyze the effect of having less characteristic modes. This may be beneficial because there are less resonances that can be excited; however, there might be consequences for the track service life as well as the performance. Part of further research also includes a study of whether the frequencies identified can be used to monitor fastening deterioration via dynamic-response-based train-borne measurements systems. Finally, a new research line would be the development of more complex models that allow the analysis of the whole fastening system, including types of clamps and elasticity of the clamps, among other parameters.

## Acknowledgments

This research was partly funded by the Collaborative Project H2020-MG-2015-2015 GA-636237b Needs Tailored Interoperable Railway—NeTIRail-INFRA. This research was also partially supported by the Dutch railway infrastructure manager ProRail.

## References

*ANSYS* [Computer software]. ANSYS, Canonsburg, PA.

*LS-Dyna* [Computer software]. Livermore Software Technology Corp., Livermore, CA.

Benson, D., and Hallquist, J. (1990). "A single surface contact algorithm for the post-buckling analysis of shell structures." *Comput. Methods Appl. Mech. Eng.*, 78(2), 141–163.

Biot, M. A. (1954). "Theory of stress-strain relations in anisotropic viscoelasticity and relaxation phenomena." *J. Appl. Phys.*, 25(11), 1385–1391.

Carrascal, I. A., Casado, J. A., Polanco, J. A., and Gutierrez-Solana, F. (2007). "Dynamic behaviour of railway fastening setting pads." *Eng. Fail. Anal.*, 14(2), 364–373.

Castellani, A., Kajon, G., Panzeri, P., and Pezzoli, P. (1998). "Elastomeric materials used for vibration isolation of railway lines." *J. Eng. Mech.*, 10.1061/(ASCE)0733-9399(1998)124:6(614), 614–621.

CEN (European Committee for Standardization). (2012). "Railway applications—Track—Test methods for fastening systems. Part 9: Determination of stiffness." *EN 13146-9+A1:2011*, Brussels, Belgium.

Chen, Y., and Huang, Y. (2003). "Dynamic characteristics of infinite and finite railways to moving loads." *J. Eng. Mech.*, 10.1061/(ASCE)0733-9399(2003)129:9(987), 987–995.

Christensen, R. (1982). *Theory of viscoelasticity: An introduction*, Academic press, New York.

Courant, R., Friedrichs, K., and Lewy, H. (1928). "Ber die partiellen differenzengleichungen der mathematischen physik." *Math. Ann.*, 100(1), 32–74.

Fermer, M., and Nielsen, J. C. O. (1995). "Vertical interaction between train and track with soft and stiff railpads—Full-scale experiments and theory." *Proc., Inst. Mech. Eng. Part F: J. Rail and Rapid Transit*, 209, 39–47.

Ferrara, R., Leonardi, G., and Jourdan, F. (2013). "A contact-area model for rail-pads connections in 2-D simulations: Sensitivity analysis of train-induced vibrations." *Veh. Syst. Dyn.*, 51(9), 1342–1362.

Ferry, J. (1961). *Viscoelastic properties of polymers*, Wiley, Hoboken, NJ.

Grassie, S. L., Gregory, R. W., Harrison, D., and Johnson, K. L. (1982). "Dynamic response of railway track to high frequency vertical excitation." *J. Mech. Eng. Sci.*, 24(2), 77–90.

Gustavson, R., and Gylltoft, K. (2002). "Influence of cracked sleepers on the global track response: Coupling of a linear track model and non-linear finite element analyses." *Proc., Inst. Mech. Eng., Part F*, 216(1), 41–51.

Ilias, H. (1999). "The influence of railpad stiffness on wheelset/track interaction and corrugation growth." *J. Sound Vib.*, 227(5), 935–948.

Kaewunruen, S., and Remennikov, A. M. (2006). "Sensitivity analysis of free vibration characteristics of an in situ railway concrete sleeper to variations of rail pad parameters." *J. Sound Vib.*, 298(1–2), 453–461.

Kassa, E., and Nielsen, J. (2008). "Dynamic interaction between train and railway turnout: Full-scale field test and validation of simulation models." *Veh. Syst. Dyn.*, 46(Suppl 1), 521–534.
Kim, E., Yang, S., and Jang, S. (2015). "Investigation and prediction of stiffness increase of resilient rail pad due to train and environmental load in high-speed railway." *2015 Joint Rail Conf.*, ASME, New York.
Knothe, K., and Wu, Y. (1998). "Receptance behaviour of railway track and subgrade." *Arch. Appl. Mech.*, 68(7–8), 457–470.
Knothe, K., and Yu, M. (2001). "Static and dynamic properties of rubber rail pads [Statische und dynamische eigenschaften von gummi-zwischenlagen fr eisenbahnschienen]." *Forsch. Ingenieurwes./Eng. Res.*, 66(6), 247–259.
Kumaran, G., Menon, D., and Nair, K. (2003). "Dynamic studies of railtrack sleepers in a track structure system." *J. Sound Vib.*, 268(3), 485–501.
Li, Z., Molodova, M., Nunez, A., and Dollevoet, R. (2015). "Improvements in axle box acceleration measurements for the detection of light squats in railway infrastructure." *IEEE Trans. Ind. Electron.*, 62(7), 4385–4397.
Maes, J., Sol, H., and Guillaume, P. (2006). "Measurements of the dynamic railpad properties." *J. Sound Vib.*, 293(3–5), 557–565.
Mandal, N. K., Dhanasekar, M., and Sun, Y. Q. (2016). "Impact forces at dipped rail joints." *Proc., Inst. Mech. Eng. Part F: J. Rail and Rapid Transit*, 230, 271–282.
Molodova, M., Li, Z., Nunez, A., and Dollevoet, R. (2014). "Automatic detection of squats in railway infrastructure." *IEEE Trans. Intell. Transp. Syst.*, 15(5), 1980–1990.
Oregui, M., de Man, A., Woldekidan, M., Li, Z., and Dollevoet, R. (2016a). "Obtaining railpad properties via dynamic mechanical analysis." *J. Sound Vib.*, 363, 460–472.
Oregui, M., Li, Z., and Dollevoet, R. (2015b). "An investigation into the modeling of railway fastening." *Int. J. Mech. Sci.*, 92, 1–11.
Oregui, M., Li, Z., and Dollevoet, R. (2015a). "Identification of characteristic frequencies of damaged railway tracks using field hammer test measurements." *Mech. Syst. Signal Process.*, 54-55, 224–242.
Oregui, M., Li, Z., and Dollevoet, R. (2016b). "An investigation into the vertical dynamics of tracks with monoblock sleepers with a 3d finite element model." *Proc., Inst. Mech. Eng. Part F*, 230(3), 891–908.
Oregui, M., Molodova, M., Nunez, A., Dollevoet, R., and Li, Z. (2015c). "Experimental investigation into the condition of insulated rail joints by impact excitation." *Exp. Mech.*, 55(9), 1597–1612.
Palsson, B., and Nielsen, J. (2015). "Dynamic vehicle-track interaction in switches and crossings and the influence of rail pad stiffness field measurements and validation of a simulation model." *Veh. Syst. Dyn.*, 53(6), 734–755.
Sadeghi, J. (2010). "Field investigation on vibration behavior of railway track systems." *Int. J. Civ. Eng.*, 8(3), 232–241.
Sol-Sánchez, M., Moreno-Navarro, F., and Rubio-Gámez, M. (2014). "Viability analysis of deconstructed tires as material for rail pads in high-speed railways." *Mater. Des.*, 64, 407–414.
Sol-Sánchez, M., Moreno-Navarro, F., and Rubio-Gámez, M. (2015). "The use of elastic elements in railway tracks: A state of the art review." *Constr. Build. Mater.*, 75, 293–305.
Thompson, D. J., Van Vliet, W. J., and Verheij, J. W. (1998). "Developments of the indirect method for measuring the high frequency dynamic stiffness of resilient elements." *J. Sound Vib.*, 213(1), 169–188.
Thompson, D. J., and Vincent, N. (1995). "Track dynamic behaviour at high frequencies, Part 1: theoretical models and laboratory measurements." *Veh. Syst. Dyn.*, 24(Suppl), 86–99.
Williams, M. L., Landel, R. F., and Ferry, J. D. (1955). "The temperature dependence of relaxation mechanisms in amorphous polymers and other glass-forming liquids." *J. Am. Chem. Soc.*, 77(14), 3701–3707.
Wu, T. X., and Thompson, D. J. (2000). "The vibration behavior of railway track at high frequencies under multiple preloads and wheel interactions." *J. Acoust. Soc. Am.*, 108(3 Part I), 1046–1053.
Zakeri, J. A., and Ghorbani, V. (2011). "Investigation on dynamic behavior of railway track in transition zone." *J. Mech. Sci. Technol.*, 25(2), 287–292.
Zakeri, J. A., and Xia, H. (2008). "Sensitivity analysis of track parameters on train-track dynamic interaction." *J. Mech. Sci. Technol.*, 22(7), 1299–1304.
Zhao, X., Li, Z., and Dollevoet, R. (2014). "Influence of the fastening modeling on the vehicle-track interaction at singular rail surface defects." *J. Comput. Nonlinear Dyn.*, 9(3), 031002.